WOOD RESEARCH doi.org/10.37763/wr.1336-4561/68.3.558571
ISSN 1336-4561 e-ISSN 2729-8906
68(3): 2023 558-571 pp.

FRACTURE TESTING OF EDGE-NOTCHED TIMBER BEAMS WITH DIFFERENT GROWTH RING ORIENTATIONS

TAMÁS KIRÁLY, ZSOLT KARÁCSONYI
UNIVERSITY OF SOPRON
HUNGARY

(RECEIVED JANUARY 2023)

ABSTRACT

The purpose of this research is to test Norway spruce specimens with different growth ring orientations weakened by edge-notch until failure. In the experiments the specimens were subjected to 3-point bending, tension and compression tests. In addition, failure mode during loading is investigated using a high-resolution camera. Based on the measurement results the correlation between latewood ratio, ultimate force, ultimate elongation/deflection, calculated moduli, growth ring orientation and diameter of the growth ring at the edge-notch were obtained. Based on the population data of the three tests conducted, only one parameter pair, namely the ratio of latewood to calculated modulus, influences the measurement results to almost the same extent. The other parameter pairs show different values and correlations.

KEYWORDS: Norway spruce (*Picea abies*), 3-point bending, tension and compression, earlywood and latewood, fracture test.

INTRODUCTION

Considering its many advantages as a natural raw material, wood is becoming increasingly popular as a building material, not only for carpentry, but also for the construction of supporting structures (Falk 2010, Raposo et al. 2017). As a result of this increasing use, wood is being used in many new applications in which it was not previously used. For this reason, the material properties of wood are studied again in order to be able to improve the design of the constructions with the determined material values using numerical methods such as the finite element method (Valipour and Crews 2011). In the last decade, it has become a trend to use wood alone or as part of a composite material (Andor et al. 2015, Raftery and Kelly 2015, Thorhallsson et al. 2017).

There is a strong relationship between density and strength of the wood (Ross 2010). Therefore, density of wood is considered the most important parameter that determines its mechanical and physical properties. It also determines the quality and use of the wood, because with a higher density it has greater strength and is therefore more suitable for use loadbearing structures. The earlywood is the portion of the growth ring that is formed during the early part of the growing season. It has a brighter color and it is less dense and weaker mechanically than latewood (Bodig and Jayne 1993). The latewood is the portion of the growth ring that is formed after the earlywood formation has ceased. It has a darker color and it is denser and stronger mechanically than earlywood. In past decades, many researchers have published on the elastic behavior of spruce timber (Keunecke et al. 2007, Dívós and Horváth 2006, Dahl and Malo 2009, Ebrahimi and Sliker 1981, Hearmon 1948, Fajdiga et al. 2019).

Wood is assumed to be a cylindrically orthotropic material with independent mechanical properties in three mutually perpendicular directions: longitudinal, radial and tangential (Szalai 2001). It is also known, that the mechanical properties of wood are greatly influenced by its anatomical structure. Considering the orientation of the annual rings is therefore of great importance and has been investigated by researchers for various applications (Fajdiga et al. 2019, Serrano and Enquist 2010, Hu et al. 2018, Belalpour et al. 2021).

The most common test to determine the strength of wood are tension, compression, static bending, indentation, shear and brittleness tests. Testing small clear specimens is the most reliable comparison of different species (Tampone 2007). In this research small and edge-notched specimens were subjected to 3-point bending-, tension- and compression tests. The measurements were filmed with a high-resolution camera and the force-displacement curves were documented as well. The measurements were evaluated and the results analyzed, which form the basis for upcoming investigations using the XFEM method and the simulation of the crack paths.

Sliker and Yu (1993) presented the elastic constants for hardwoods from measurement data by carrying out plate and tension tests. Liu (2002) presented a stress analysis of the off-axis tension test using an orthotropic material model. The off-axis tension test is attractive because of its economy and ease of application. Liu and Ross (2005) estimated the compressive modulus in radial direction with his verified shear modulus model, based on the weak band theory (Bodig 1965). In the radial direction, earlywood and latewood bands are arranged in series and both bands carry the same load, but the latewood deforms much less. The failure occurs therefore in the weakest earlywood band. To compare the tested specimens in this research, the most obvious choice was to determine the elastic modulus. In addition, the specimens were weighed and photographed from all sides before testing, in order to estimate the latewood ratio (Király et al. 2023). A digital camera was used for these tests, in order to obtain the deformation field and the path of the crack.

MATERIAL AND METHODS

Measurement set-up

All the experiments with timber beams were conducted in a laboratory accredited for timber structural testing. The tests were carried out in accordance with ASTM D198-02. All of

the specimens were sawn of Norway spruce (*Picea abies*) and dried to a moisture content of 12%. The experiments were carried out at a room temperature of 20°C. The equipment used for the tests consists of a material testing machine (Tinius Olsen H10KT), an LED lamp (Jinbei EF-200) as an additional light source focused on the sample, a camera with Red Dragon 5K sensor and Samyang 3.1/100 mm optics. The displacement was controlled at a constant speed during a test. The feed rates of the specimens were documented in the range of 0,1 – 5 mm/min.

The orientation of growth rings in the specimens are aligned in an angle α between 0 to 90 degrees as shown in Fig. 1. The value of α is 0, if the grains are perpendicular to the longitudinal axis of the specimen and 90, if the grains are parallel. In the population, the mode of failure is the same between similar specimens, but the cracking may vary depending on the orientation of the growth rings. The diameter of the growth rings (dGR) at the location of the edge-notch is also documented in the table of specimen data (Tabs. 1-3).

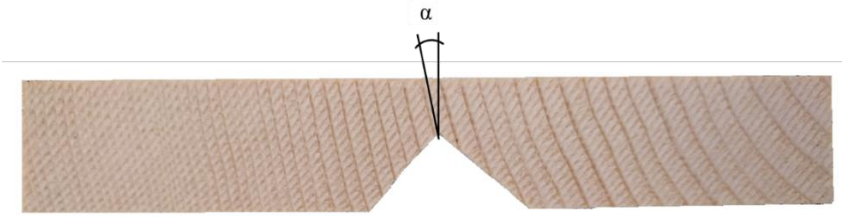

Fig. 1: Growth ring orientation (α) in the specimen at the notch.

The proportions of latewood and earlywood in the specimens are determined using a photo-analytical algorithm. As suggested in Király et al. (2023), the volume ratio of the latewood in the specimen can be estimated from its surface ratio.

3-point bending tests

This test method covers the determination of the flexural properties of structural beams (ASTM D198-02). The flexural modulus E_f (also called bending modulus) is a property that is computed as the ratio of stress to strain in flexural deformation and it describes the tendency for a material to resist bending (Yoshihara et al. 1998). As bending occurs in the specimen, its top surface experiences compression while the bottom side experiences tension. Calculation of flexural modulus E_f of the 3-point bending tests for rectangular shaped specimens with constant cross-section, where "u" stands for the maximal deflection of the beam under the load "F":

$$E_f = \frac{F \cdot L^3}{u \cdot 4W \cdot H^3} \tag{1}$$

Because of the edge-notch, the cross-section and also the moment inertia of area must be considered as variable. As a conservative simplification, the cross section with the edge-notch is considered with a rectangular cross section with height "h" (Fig. 2):

$$I_1 = \frac{W \cdot H^3}{12} \quad for\ 0 \le x \le l \tag{2}$$

$$I_2 = \frac{W \cdot h^3}{12} + \left(\frac{H-h}{2}\right)^2 \cdot W \cdot H \quad for\ l < x \le L/2 \tag{3}$$

The Eq. 1 can be extended in the following way, to get more accurate results:

$$E_f = \frac{F}{u \cdot I_2}\left(\frac{L^3}{48} + \frac{l^3}{3}\right) + \frac{F}{u \cdot I_1} \cdot \frac{l^3}{6} \quad (4)$$

The parameters of the specimens used for the 3-point bending test are as shown in Fig. 2 and Tab. 1.

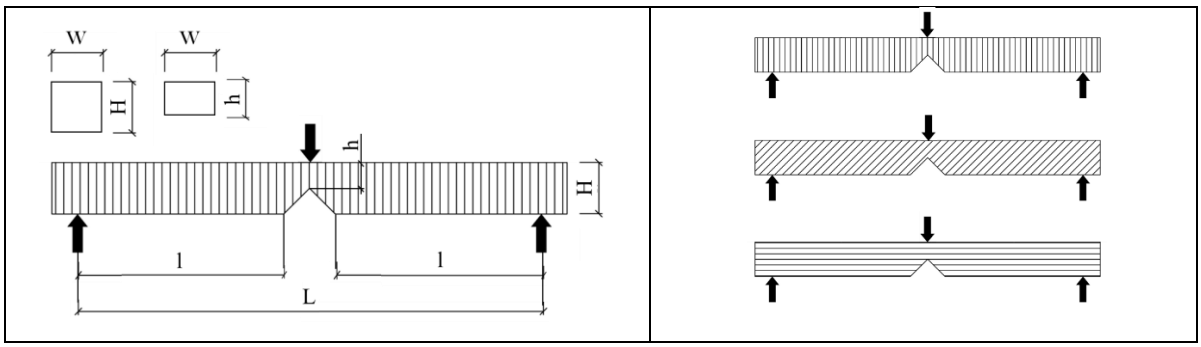

Fig. 2: Schematic of specimen types with different growth ring orientations used for the 3-point bending test: L – span length of specimen, W – width of specimen, h – height at the notch, l – distance between support and edge-notch.

Tab. 1: Data of specimens used for the 3-point bending test.

Nº	**L** (mm)	**W** (mm)	**h** (mm)	**α** (deg)	**Weight** (g)	**Latewood ratio** (%)	**Feed rate** (mm/min)	**dGR** (mm)
HA01	110.0	20.1	8.9	28.6	18.95	17.4	0.1	194.4
HA02	110.0	20.0	9.0	16.2	18.16	15.5	0.1	167.5
HA03	110.0	20.0	8.8	24.0	18.69	18.3	0.1	156.7
HA04	110.0	20.0	8.9	23.2	19.05	12.7	0.1	147.4
HA05	50.0	20.6	9.7	3.0	14.77	11.5	0.5	70.4
HA06	50.0	20.6	9.5	6.7	14.65	12.1	0.5	68.4
HA07	50,0	20.7	10.5	2.5	14.88	16.0	0.5	66.6
HA08	110.0	20.3	9.4	90.0	24.60	18.2	1.0	92.0
HA09	110.0	20.3	9.4	90.0	24.61	16.0	1.0	94.3

Tension tests

This test method covers the determination of the tensile properties of structural elements made primarily of lumber equal to and greater than nominal 1 inch (19 mm) thick (ASTM D198-02). The specimen is clamped at the extremities of its length and subjected to a tensile load so that in sections between clamps the tensile forces shall be axial and generally uniformly distributed throughout the cross-sections without flexure along its length.

Wood has a moderately high tensile strength and requires a high clamping force device to secure it. Wood is also moderately soft, which presents a challenge for conventional mechanical vices. The basic formula for obtaining the elastic tensile modulus E_t in case of tension:

$$E_t = \frac{\sigma}{\epsilon} = \frac{F/A}{dL/L} \quad (5)$$

Because of the edge-notch, the cross-section must be considered as variable. Elongation dL of the specimen, can be considered as springs connected in series. The total elongation corresponds to the sum of the length changes of the individual sections of the specimen:

$$dL = 2 \cdot dL_1 + dL_2 = \frac{F}{E_t} \cdot \left(\frac{2 \cdot l}{A_1} + \frac{L - 2 \cdot l}{A_2}\right) \quad (6)$$

The cross-sections of the considered segments are:

$$A_1 = W \cdot H \quad (7)$$

$$A_2 = W \cdot h \quad (8)$$

The Eq. 5 is therefore extended in the following way:

$$E_t = \frac{F}{dL} \cdot \left(\frac{2 \cdot l}{A_1} + \frac{L - 2 \cdot l}{A_2}\right) \quad (9)$$

The parameters of the specimens used for the tension test are as shown in Fig. 3 and Tab. 2.

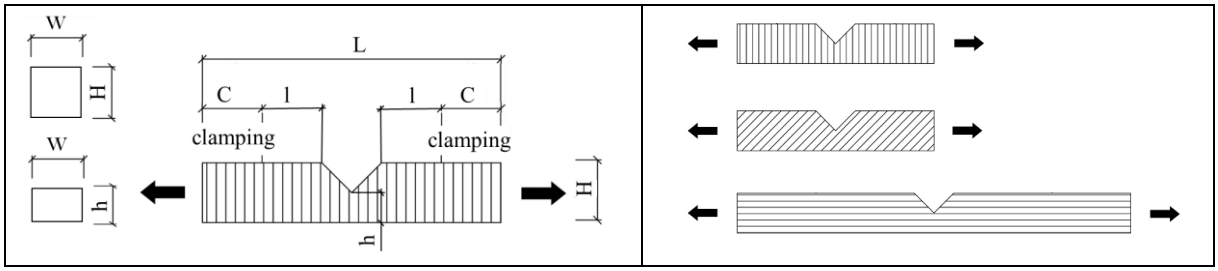

Fig. 3: Schematic of specimen types with different growth ring orientations used for the tension test: L – free length of specimen, W – width of specimen, C – length of the clamping, h – height at the notch, l – distance between clamping and edge-notch.

Tab. 2: Data of specimens used for the tension test.

Nº	**L** (mm)	**C** (mm)	**W** (mm)	**h** (mm)	**α** (deg)	**Weight** (g)	**Latewood ratio** (%)	**Feed rate** (mm/min)	**dGR** (mm)
HU01	160.0	40.0	19.9	13.1	90.0	31.29	11.3	0.1	56.7
HU02	160.0	40.0	20.0	12.0	90.0	32.67	13.2	0.1	95.0
HU03	160.0	40.0	20.1	13.1	33.4	32.23	12.4	0.1	124.9
HU04	80.0	20.0	20.2	8.5	22.4	18.85	13.2	0.1	138.8
HU05	80.0	20.0	20.5	9.8	3.9	14.55	14.2	0.1	140.0
HU06	80.0	20.0	20.5	9.7	9.3	14.64	14.0	0.1	134.0
HU07	80.0	20.0	20.6	9.1	11.8	14.63	15.1	0.1	114.7
HU08	160.0	40.0	20.2	10.3	90.0	24.17	16.3	0.1	145.6
HU09	160.0	40.0	20.0	10.0	90.0	24.11	17.2	1.0	148.8

Compression tests

This test method covers the determination of the compressive properties of elements taken from structural members made of solid wood, when such an element has a slenderness ratio (length to least radius of gyration) of less than 17 (ASTM D198-02). If the slenderness ratio is less than 17, the specimen is considered small and no lateral support is required. The elastic compression modulus E_c can be obtained by using Eq. 9.

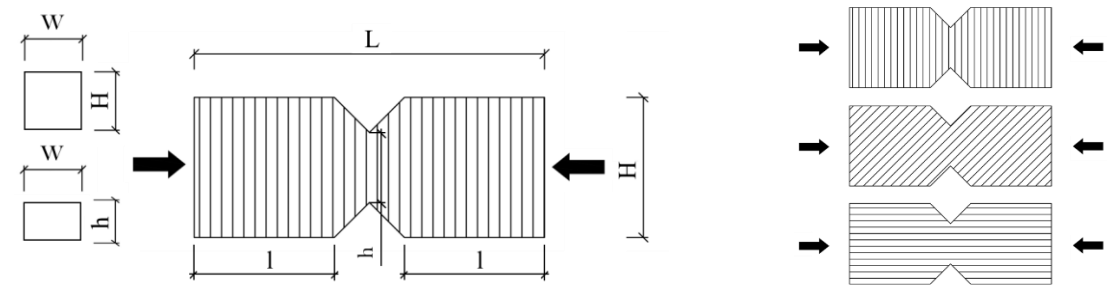

Fig. 4: Schematic of specimen types with different growth ring orientations used for the compression test: L – length of specimen, W – width of specimen, h – height at the notch, l – distance between support and edge-notch.

Tab. 3: Data of specimens used for the compression test.

Nº	**L** (mm)	**W** (mm)	**h** (mm)	**α** (deg)	**Weight** (g)	**Latewood ratio** (%)	**Feed rate** (mm/min)	**dGR** (mm)
NY01	100.0	39.6	15.7	26.2	60.56	10.8	1.0	174.6
NY02	100.0	39.8	15.7	27.1	60.91	12.3	5.0	157.2
NY03	100.0	40.5	19.8	90.0	70.44	18.1	5.0	129.7
NY04	100.0	40.5	19.4	90.0	71.48	21.3	5.0	112.8
NY05	100.0	40.5	19.1	13.7	70.38	18.4	5.0	132.4
NY06	100.0	40.4	19.3	1.4	71.97	19.3	5.0	126.1
NY07	100.0	40.4	18.8	90.0	69.76	18.2	5.0	119.4
NY08	100.0	40.5	19.0	90.0	68.88	21.1	5.0	122.0
NY09	100.0	40.5	19.7	7.0	72.23	19.1	5.0	122.1

RESULTS AND DISCUSSION

Experiment results

In examining the fracture of wood at the macro-level, no attempt is made to investigate the failure at lower levels of material structure, only the behavior under load. The measurement method is responsible for the nonlinear initial phase (Bodig 1965). There are always surface irregularities, especially in wood. The force applied is proportional to the size of the contact area, which may be smaller in the initial stage. In case of the tension test, also a minimal sliding in the clamping may occur at the start of the measurement (most striking example is HU2 in Fig. 5b.

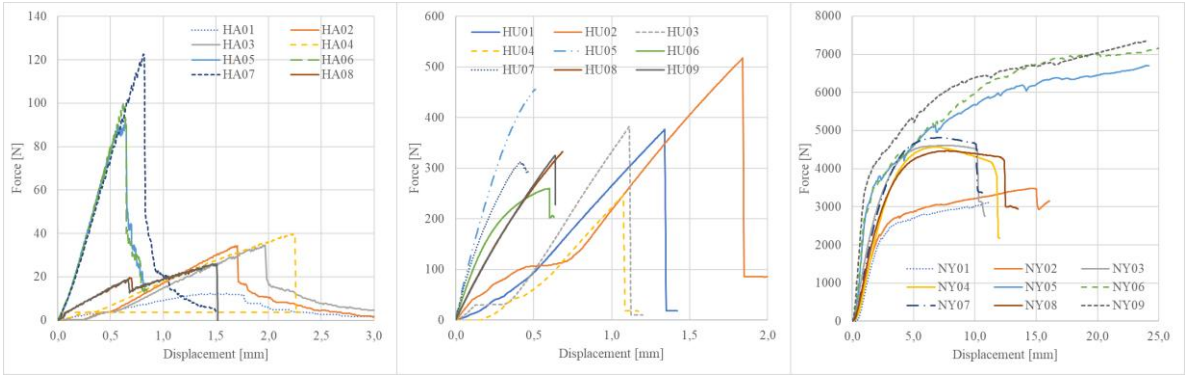

a) *b)* *c)*

Fig. 5: Force-displacement diagrams: a) 3-point bending test, b) tension test, c) compression test.

In the 3-point bending test 9 specimens were successfully tested (Tab. 4). During the measurement, the force-displacement diagram was documented, from which the flexure modulus can be calculated. With the video recording the failure mode as well as the crack path was captured. After the first crack appears, the resistance of the specimen drops rapidly. The weakened cross-section yields and the crack grows proportionally with the feed through the specimen in the direction of the punch. Depending on the orientation of the growth rings, the typical failure is cross-grain tension (grain alignment perpendicular) and brash tension (grain alignment parallel), see Fig. 6.

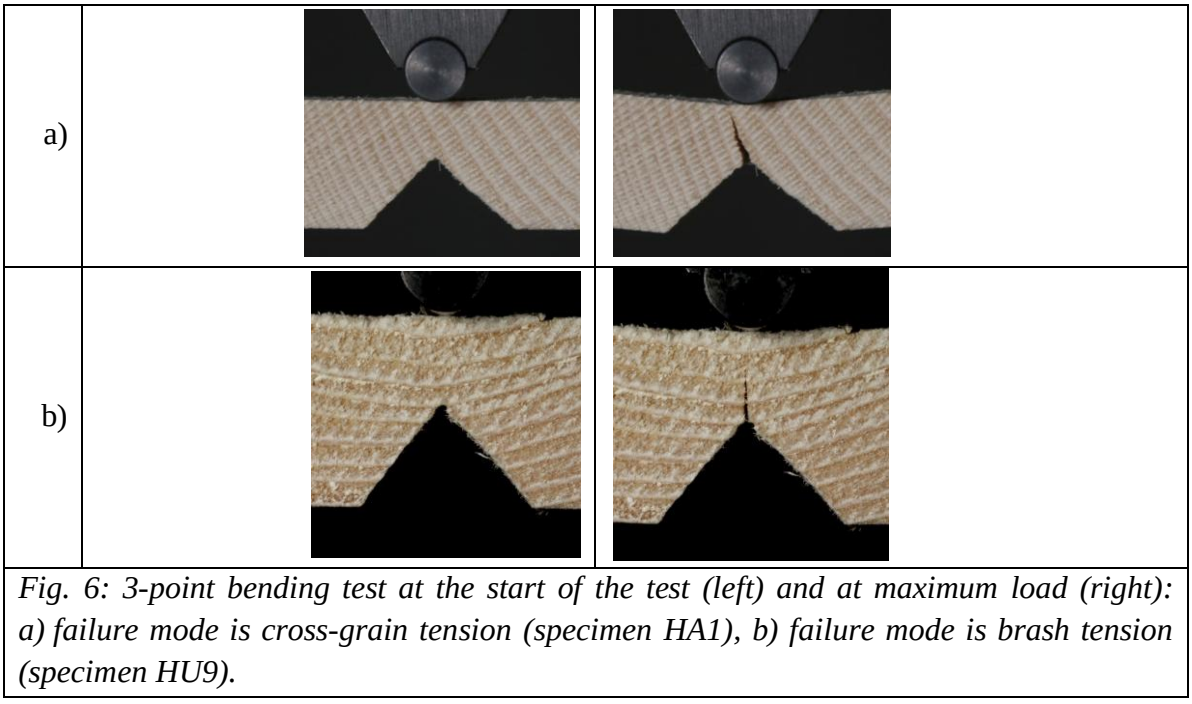

Fig. 6: 3-point bending test at the start of the test (left) and at maximum load (right): a) failure mode is cross-grain tension (specimen HA1), b) failure mode is brash tension (specimen HU9).

Tab. 4: Experiment results of the 3-point bending test.

№	**L** (mm)	**α** (deg)	**dGR** (mm)	**Ultimate force** (N)	**Ultimate deflection** (mm)	**Lin. flexure modulus** (MPa)	**Failure mode**
HA01	130.0	28.6	194.4	12.0	1.6	63.7	cross-grain tension
HA02	130.0	16.2	167.5	34.3	1.7	139.7	cross-grain tension
HA03	130.0	24.0	156.7	34.7	2.0	127.7	cross-grain tension
HA04	130.0	23.2	147.4	39.7	2.2	129.0	cross-grain tension
HA05	80.0	3.0	70.4	91.0	0.6	54.3	cross-grain tension
HA06	80.0	6.7	68.4	99.7	0.6	56.3	cross-grain tension
HA07	80.0	2.5	66.6	122.6	0.8	45.3	cross-grain tension
HA08	130.0	90.0	92.0	24.0	1.3	186.7	simple- and brash tension
HA09	130.0	90.0	94.3	26.0	1.5	189.4	brash tension
Average	***113.3***	***31.6***	***117.6***	***53.8***	***1.4***	***110.2***	
St. dev.	***23.6***	***32.5***	***46.2***	***37.4***	***0.5***	***53.8***	

In the tensile test 9 specimens were tested (Tab. 5). As for the bending test, the same parameters were documented. The crack grows through rapidly in the weakened cross-section. The 100 Hz frame rate of the camera is not sufficient for the crack growth to be resolved as for the 3-point bending test. Usually, 2-3 frames are recorded of the crack growth until complete

failure. Depending on the orientation of the growth rings, the typical failure is brittle tension (grain alignment perpendicular) and shearing along the growth ring (grain alignment parallel), see Fig. 7.

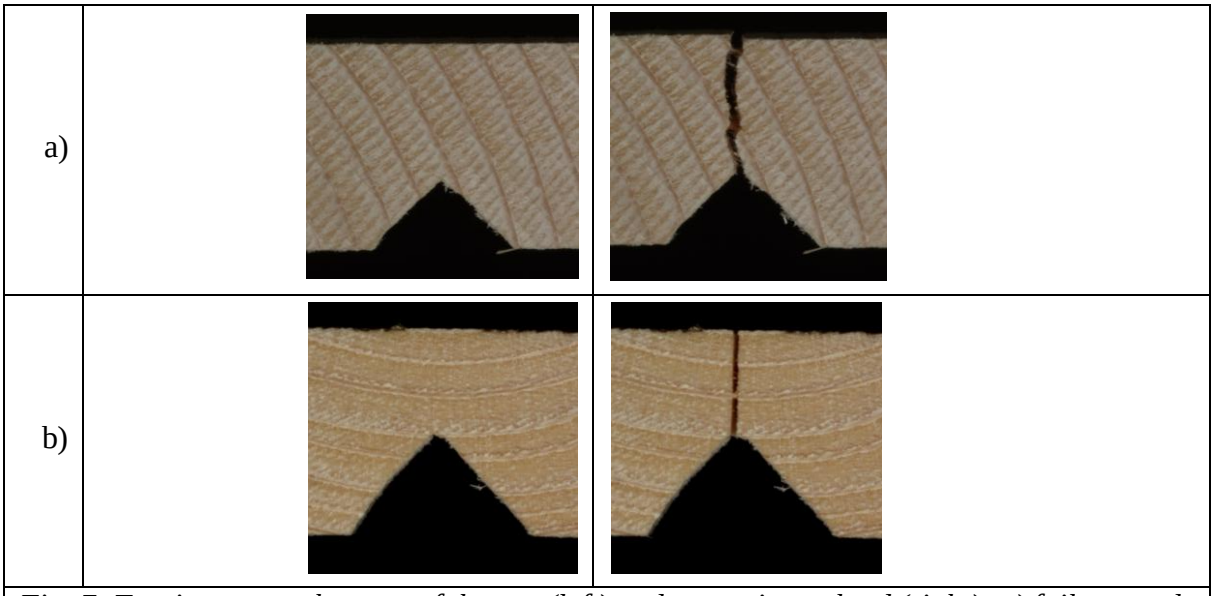

Fig. 7: Tension test at the start of the test (left) and at maximum load (right): a) failure mode is a combination of shearing along the growth ring and tension failure of earlywood (specimen HU3), b) failure mode is brittle tension (specimen HU8).

Tab. 5: Experiment results of the tension test.

№	**L** (mm)	**α** (deg)	**dGR** (mm)	**Ultimate force** (N)	**Ultimate elongation** (mm)	**Tension modulus** (MPa)	**Failure mode**
HU01	160.0	90.0	174.6	376.4	1.3	80.0	tension parallel to grain: brittle tension
HU02	160.0	90.0	157.2	517.5	1.8	83.9	tension parallel to grain: brittle tension
HU03	160.0	33.4	129.7	382.4	1.1	91.6	tension perpendicular to the grain: combination of shearing along the growth ring and tension failure of earlywood
HU04	80.0	22.4	112.8	247.0	1.1	38.4	tension perpendicular to the grain: shearing along the growth ring
HU05	80.0	3.9	132.4	455.4	0.5	284.7	tension perpendicular to the grain: shearing along the growth ring
HU06	80.0	9.3	126.1	259.4	0.6	197.9	tension perpendicular to the grain: shearing along the growth ring
HU07	80.0	11.8	119.4	313.2	0.4	251.8	tension perpendicular to the grain: shearing along the growth ring
HU08	160.0	90.0	122.0	332.4	0.7	225.0	tension parallel to grain: brittle tension
HU09	160.0	90.0	122.1	325.6	0.6	224.9	tension parallel to grain: brittle tension
Average	***124.4***	***49.0***	***122.1***	***356.6***	***0.9***	***164.2***	
St. dev.	***39.8***	***37.5***	***28.0***	***82.7***	***0.4***	***85.2***	

Also, in the compression test 9 specimens were tested (Tab. 6). The documented parameters are the same, as in case of the other tests. Crack growth (in the macro range) is a slow process and occurs after a large elastoplastic deformation. The force-displacement curves always show a bend after the compressive force increases slowly. When the specimen

buckles laterally, the force that can be applied decreases, as for example in NY04, NY07, NY09. Depending on the orientation of the growth rings, the typical failure is the collapse of earlywood layers in the middle of the specimen combined with shearing along the side (grain alignment perpendicular) and crushing and splitting (grain alignment parallel), see Fig. 8.

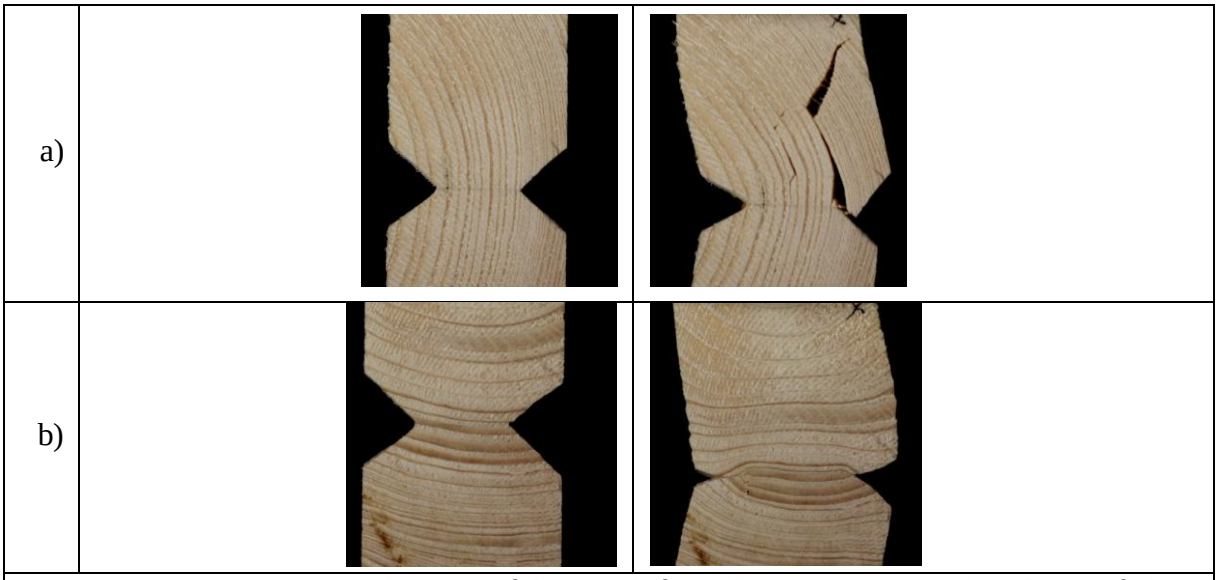

Fig. 8: Compression test at the start of the test (left) and at maximum load (right): a) failure mode is crushing and splitting (specimen NY3), b) failure mode is collapse of earlywood layers (specimen NY6).

Tab. 6: Experiment results of the compression test.

Nº	**L** (mm)	**α** (deg)	**dGR** (mm)	**Ultimate force** (N)	**Ultimate elongation** (mm)	**Compression modulus** (MPa)	**Failure mode**
NY01	100.0	26.2	174.6	3128.0	11.3	78.2	compression perpendicular to grain: in the middle earlywood layers collapse, while on the side shearing along the growth ring
NY02	100.0	27.1	157.2	3484.0	14.8	97.5	compression perpendicular to grain: in the middle earlywood layers collapse, while on the side shearing along the growth ring
NY03	100.0	90.0	129.7	4610.0	8.0	128.9	compression parallel to the grain: crushing and splitting
NY04	100.0	90.0	112.8	4565.0	7.0	87.0	compression parallel to the grain: crushing and splitting
NY05	100.0	13.7	132.4	6705.0	24.2	196.2	compression perpendicular to grain: earlywood layers collapse
NY06	100.0	1.4	126.1	7417.5	28.6	209.8	compression perpendicular to grain: earlywood layers collapse
NY07	100.0	90.0	119.4	4810.0	7.4	111.4	compression parallel to the grain: crushing and splitting
NY08	100.0	90.0	122.0	4465.0	7.9	102.6	compression parallel to the grain: crushing and splitting
NY09	100.0	7.0	122.1	7357.5	24.0	271.4	compression perpendicular to grain: earlywood layers collapse
Average	***100.0***	***48.4***	***132.9***	***5171.3***	***14.8***	***142.6***	
St. dev.	***0.0***	***38.0***	***18.9***	***1509.6***	***8.1***	***63.3***	

Correlation of the different parameters of the specimen

In the experiments, the specimens were subjected to 3-point bending-, tension- and compression tests. In each type of test, 9 specimens with different orientation and diameter of the growth rings at the edge-notch were investigated.

Based on the measurement results (Tab. 4, Tab. 5 and Tab. 6) the correlation between the variables can be calculated.

Tab. *7* shows the correlation of the variables growth ring orientation (α), the diameter of the growth ring at the edge-notch (dGR), latewood ratio (LWr), ultimate force (F_u), ultimate elongation/deflection (u_u) and the calculated moduli (E_f , E_t, E_c). The correlation coefficient (r_{xy}) indicates the strength of the linear relationship between the variables:

$$r_{xy} = \frac{\sum(x_i-\overline{x})(y_i-\overline{y})}{\sqrt{\sum(x_i-\overline{x})^2\sum(y_i-\overline{y})^2}} \; ; \; -1 < r_{xy} < 1 \tag{8}$$

A negative value of r_{xy} means negative correlation, which means that the variables tend to move in opposite direction. The value 0 means no correlation at all. A positive correlation means, that the variables move in the same direction.

Tab. 7: Correlation of the variables based on the measurement data.

Test type	**x: α y: F_u**	**x: α y: u_u**	**x: α y: $E_{f/t/c}$**	**x: LWr y: F_u**	**x: LWr y: u_u**	**x: LWr y: $E_{f/t/c}$**	**x: dGR y: F_u**	**x: dGR y: u_u**	**x: dGR y: $E_{f/t/c}$**
3-p. bend. tests	-0,337	-0,685	0,755	-0,554	-0,619	0,446	-0,737	0,389	-0,941
tension test	0,311	0,517	-0,254	-0,244	-0,629	0,715	-0,378	-0,628	0,480
compr. test	-0,506	-0,900	-0,638	0,555	0,031	0,335	-0,542	0,008	-0,338

Strength of relationship	-0,1 to 0,1	-0,3 to -0,1 or 0,1 to 0,3	-0,5 to -0,3 or 0,3 to 0,5	-1,0 to -0,5 or 1,0 to 0,5
	very weak	weak	moderate	strong

From that we can conclude that based on the population data of the 3 tests considered, only one parameter pair, the latewood ratio versus the calculated moduli, influences the measurement results to almost the same extent. The other parameter pairs show different values and correlations. This means that the corresponding measurements are can be sensitive to changes in certain parameters. It can be clearly seen that in the compression test, the elongation in relation to the diameter of the growth rings at the edge-notch and to the latewood ratio has a correlation value close to zero, while for the bending test and tension test these parameter pairs have a high impact.

The growth ring orientation has a great influence on the load-bearing capacity and also on the ultimate elongation/deflection. For the calculation of the correlation of F_u and u_u, the measurement values were normalized to eliminate the influence of the length of the specimens. In case of the 3-point bending test and compression test lower values of α lead to a higher ultimate force and ultimate elongation /deflection. Although these specimens with high α values (grains are parallel) have a higher calculated modulus of elasticity before the first sign of the material degradation, the crack in the edge notch occurs earlier in the bending tests and splitting occurs earlier in the compression tests, which affects the load-carrying capacity.

In the compression tests, the collapse of the earlywood layers delays buckling because the edge notch zone is squeezed and the specimen shortens.

A higher latewood ratio (LWr) does not necessarily lead to higher ultimate load F_u and calculated moduli (E_f, E_t, E_c), while these are more influenced by the orientation of the growth rings in the specimens. The largest positive influence of higher LWr values on the calculated moduli is seen in the compression tests. The LWr in the specimens tested is between 10,8% and 21,3% with an average of 15,7% and standard deviation of 3,0%.

The smaller diameter of the growth ring at the edge-notch (dGR) in most cases causes higher F_u values in the tested population, mainly because the crack has to propagate through several earlywood and latewood layers instead of spreading in just one layer. In case of the 3-point bending tests the correlation between dGR and E_f shows, that smaller diameters lead to higher flexural modulus. This is only the case, because in the population the specimens with the growth ring orientations parallel to the grains ($\alpha = 90°$) have tendentially smaller dGR values. In this case, population size leads to a misinterpretation of the correlation between variables. In practice, as in the tension tests, a larger E modulus is obtained with a larger dGR and parallel to the grain orientation. In case of the compression test with parallel to the grain orientation splitting occurs earlier if the dGR values are higher. The diameter of the growth ring in the specimens tested are between 56,7 mm and 194,4 mm with an average of 131,1 mm and standard deviation of 28,9 mm.

CONCLUSIONS

In the experiment edge-notched Norway spruce specimens were tested until failure with 3-point bending-, tension- and compression tests. In each type of test 9 samples with different growth ring orientation were tested. The results of individual test types are summarized in Tab. *4*, Tab. 5 and Tab. 6, respectively.

For the measurement results, the correlations of the different variables were calculated (

Tab. *7*). The correlation table helps to understand the relevant variables for the different types of tests, i.e., a higher proportion of latewood does not necessarily lead to a higher load-bearing capacity, while this is more influenced by the orientation of the growth rings in the specimen.

The experiments were recorded with a high-resolution highspeed camera, where the failure mode and the crack path are clearly visible. The video documentation of the crack path is required for the upcoming investigation, where the failure of the specimens will be investigated with XFEM. The specimens of the 3-point bending tests and tension tests fail with brittle fracture. This can be seen in the curves in Fig. 5. The failure mode of these tests can be reproduced and examined by XFEM. However, for the compression test, a horizontal plateau in the force curve is observed, indicating a large elastoplastic deformation. This cannot be well investigated by XFEM using the principle of linear elastic fracture mechanics, since the extent of elastoplastic deformation, plasticity that prevails in a large area in the specimen and failure behavior cannot be described by this method. There are publications that investigate the failure

behavior at cell level (Lukacevic et al. 2015), but there have been no breakthroughs at the macro level while considering the growth ring pattern in the specimen.

REFERENCES

1. ASTM D198-02: Standard Test Methods of Static Tests of Lumber in Structural Sizes.
2. Andor, K., Lengyel, A., Polgár, R., Fodor, T., Karácsonyi, Z., 2015: Experimental and statistical analysis of spruce timber beams reinforced with CFRP fabric. Construction and Building Material 99: pp. 200–207.
3. Belalpour Dastjerdi, P.; Landis, E.N., 2021: Growth Ring Orientation Effects in Transverse Softwood Fracture. MDPI Materials 2021, Volume 14, article number 5755.
4. Bodig, J., Jayne, B.A., 1993: Mechanics of Wood and Wood Composites. Rep. Edition, Krieger Publishing: pp. 291-305.
5. Bodig., J., 1965: The effect of anatomy on the initial stress-strain relationship in transverse compression. Forest Products Journal 15(5): pp. 197-202.
6. Dahl, K.B., Malo, K.A., 2009: Linear shear properties of spruce softwood. Wood Science and Technology, 43, pp. 499-525.
7. Dívós, F., Horváth, M., 2006: Faanyag rugalmas állandóinak dinamikus meghatározása, összehasonlítása. [Dynamic determination and comparison of elastic constants of wood.] Faipar, 54, pp. 3-8.
8. Ebrahimi, G., Sliker, A., 1981: Measurement of shear modulus in wood by a tension test. Wood Science, 13, pp. 171-176.
9. Fajdiga, G., Rajh, D., Nečemer, B., Glodež, S., Šraml, M., 2019: Experimental and Numerical Determination of the Mechanical Properties of Spruce Wood. MPDI Forest 10(12) 2019, article number 1140.
10. Falk, R.H., 2010: Wood handbook: Wood as an engineering material: chapter 1. Centennial ed. General technical report FPL, WI: U.S. Dept. of Agriculture, Forest Service, Forest Products Laboratory, pp. 1.1-1.6
11. Hearmon, R.F.S., 1948: The Elasticity of wood and plywood – Forest Product Research, Special Report No. 7; London: His Majesty's Stationery Office, pp. 5-57.
12. Hu, M., Olsson, A., Johansson, M., Oscarsson, J., 2018: Modelling local bending stiffness based on fibre orientation in sawn timber. European Journal of Wood and Wood Products 76: pp. 1605–1621.
13. Keunecke, D., Sondereeger, W., Pereteanu, K., Lüthi, T., Niemz, P., 2007: Determination of Young's and shear moduli of common yew and Norway spruce by means of ultrasonic waves. Wood Sci Technology, 41, pp. 309-327.
14. Király, T., Karácsonyi, Zs., Polgár, R., 2023: Modeling the earlywood and latewood growth rings of Norway spurce timber beams for finite element calculation. Wood Research 68 (1), pp. 28-43.
15. Liu, J.Y., 2002: Analysis of off-axis tension test of wood specimens. Wood and Fiber Science, 34, pp. 205-211.
16. Liu, J.Y., Ross, R.J., 2005: Relationship between radial compressive modulus of elasticity and shear modulus of wood. Wood and Fiber Science, 37, pp. 201-206.

17. Lukacevic, M., Füssl, J. and Lampert, R., 2015: Failure mechanisms of clear wood identified at wood cell level by an approach based on the extended finite element method. Engineering Fracture Mechanics 144: pp. 158-175.
18. Raftery, G.M., Kelly, F., 2015: Basalt FRP rods for reinforcement and repair of timber. Composites Part B: Engineering 70: pp. 9–19.
19. Raposo, P., Correia, J., Sousa, D., Salavessa, M., Reis, C., Oliveira, C. and De Jesus, A., 2017: Mechanical Properties of Wood Construction Materials from a Building from the 19th Century, Procedia Structural Integrity, 5, pp. 1097-1101.
20. Ross, R.J., 2010: Wood handbook: Wood as an engineering material. Centennial ed. General technical report FPL-GTR-190. Madison WI, U.S. Dept. of Agriculture. Forest Service, Forest Products Laboratory, pp. 509.
21. Serrano, E., Enquist, B., 2010: Compression strength perpendicular to grain in cross-laminated timber (CLT). 11th World Conference on Timber Engineering 2010, WCTE 2010, Volume 1, pp. 441-448.
22. Sliker, A., Yu, Y., 1993: Elastic constants for hardwoods measured from plate and tension tests. Wood and Fiber Science 25, pp. 8-22.
23. Szalai, J. (2001): A faanyag és faalapú anyagok anizotrop rugalmasság- és szilárdságtana – Hillebrand Nyomda. [Anisotropic elasticity and strength of wood and wood-based materials - Hillebrand Printing Company.] Sopron, pp. 80-203.
24. Tampone, G., 2007: Mechanical Failures of the Timber Structural Systems, ICOMOS IWC, XVI International Symposium.
25. Thorhallsson, E.R., Hinriksson, G.I., Snæbjörnsson, J.T., 2017: Strength and stiffness of glulam beams reinforced with glass and basalt fibres. Composites Part B: Engineer 115: pp. 300–307.
26. Valipour, H.R., Crews, K., 2011: Efficient finite element modelling of timber beams strengthened with bonded fibre reinforced polymers. Construction and Building Material 25: pp. 3291–3300.
27. Yoshihara, H., Kubojima, Y., Nagaoka, K., 1998: Measurement of the shear modulus of wood by static bending tests. J Wood Sci 44, pp. 15–20.

TAMÁS KIRÁLY*, ZSOLT KARÁCSONYI
UNIVERSITY OF SOPRON
INSTITUTE FOR APPLIED MECHANICS AND STRUCTURES
BAJCSY-ZSILINSZKY U. 4.
H-9400 SOPRON
HUNGARY
*Corresponding author: tamas.kiraly1990@gmail.com